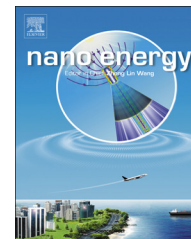




Available online at [www.sciencedirect.com](http://www.sciencedirect.com)

ScienceDirect

journal homepage: [www.elsevier.com/locate/nanoenergy](http://www.elsevier.com/locate/nanoenergy)



RAPID COMMUNICATION

# TiO<sub>2</sub>(R)/VO<sub>2</sub>(M)/TiO<sub>2</sub>(A) multilayer film as smart window: Combination of energy-saving, antifogging and self-cleaning functions



Jianyun Zheng<sup>a,b</sup>, Shanhu Bao<sup>a</sup>, Ping Jin<sup>a,c,\*</sup>

<sup>a</sup>State Key Laboratory of High Performance Ceramics and Superfine Microstructure, Shanghai Institute of Ceramics, Chinese Academy of Sciences, Dingxi Rd. 1295, Changning District, Shanghai 200050, China

<sup>b</sup>Graduate School of Chinese Academy of Sciences, Beijing 100049, China

<sup>c</sup>Materials Research Institute for Sustainable Development, National Institute of Advanced Industrial Science and Technology (AIST), 2266-98 Shimoshidami, Moriyama-ku, Nagoya 463-8560, Japan

Received 24 August 2014; received in revised form 22 September 2014; accepted 23 September 2014

Available online 27 October 2014

## KEYWORDS

TiO<sub>2</sub>(R)/VO<sub>2</sub>(M)/  
TiO<sub>2</sub>(A) multilayer;  
Smart window;  
Antifogging;  
Self-cleaning;  
Saving energy

## Abstract

A novel Multifunctional TiO<sub>2</sub>(R)/VO<sub>2</sub>(M)/TiO<sub>2</sub>(A) multilayer film is designed and deposited by medium frequency reactive magnetron sputtering. An exciting fact that the antifogging, self-cleaning and energy-saving effects are integrated into the multilayer film could offer significant potential for wider applications of smart window. Thereinto, the bottom TiO<sub>2</sub> layer with rutile phase plays an important role in the formation of monoclinic phase of VO<sub>2</sub> layer and serves as an antireflection layer. Then, the VO<sub>2</sub> layer with dominant monoclinic phase performs an automatic solar/heat control for saving energy. Finally, the top TiO<sub>2</sub> layer containing a mixed phase of anatase and rutile displays the remarkable photocatalytic and photoinduced properties. According to optical tests, the multilayer film shows satisfactory optical properties with an excellent solar regulation efficiency ( $\Delta T_{\text{sol}}=10.2\%$ ) and an applicable luminous transmittance ( $T_{\text{lum-L}}=30.1\%$ ) in a low-temperature state. In addition, the multilayer film implements a photoinduced super-hydrophilicity ( $\sim 2.1^\circ$ ) through UV-irradiation, resulting in an antifogging effect. A high level of photocatalytic activity is detected on the surface of the multilayer film through degradation of stearic acid and rhodamine B.

© 2014 Elsevier Ltd. All rights reserved.

\*Corresponding author at: State Key Laboratory of High Performance Ceramics and Superfine Microstructure, Shanghai Institute of Ceramics, Chinese Academy of Sciences, Dingxi Rd. 1295, Changning District, Shanghai 200050, China. Tel.: +86 21 69906208.

E-mail address: [p-jin@mail.sic.ac.cn](mailto:p-jin@mail.sic.ac.cn) (P. Jin).

## Introduction

Windows capable of regulating solar/heat transmission for energy efficiency and comfort are called smart. [1,2] Smart windows have the potential to moderate the energy consumption of buildings, which is almost the equivalent of 30–40% of the primary energy used in worldwide. [3,4] Among the various types of chromogenic materials, thermochromic materials have attracted the attention of researchers and been the subject of extensive studies for applications to smart windows. [5–7] The most widely studied thermochromic material as smart window is VO<sub>2</sub> with the monoclinic (M) phase (shown as VO<sub>2</sub>(M)), which is able to execute a reversible transition at a phase-transition temperature ( $T_c \approx 68$  °C): below  $T_c$  the material is monoclinic, insulating and quite infrared transparent (VO<sub>2</sub>(M)), and above  $T_c$  it is tetragonal, metallic and infrared reflecting (VO<sub>2</sub>(R)). [8] The idea of using VO<sub>2</sub>(M) for a smart window can be realized because  $\sim 40$  °C of  $T_c$  has been attained by various dopings, in which the replacement of V<sup>4+</sup> by a small amount of penta- or hexavalent ions seems to be the most effective. [9,10] Currently, to fabricate VO<sub>2</sub>(M) based films, several methods have been applied, such as wet chemical approaches [11,12], chemical vapor deposition (CVD) [13–15], pulsed laser deposition (PLD) [16,17] and magnetron sputtering (MS) [18–20].

As is well known, the windows of the buildings and vehicles always need to be washed by the cleaners using detergents. With respect to these cleaning processes, there are two disadvantageous factors: (1) producing additional pollutants from the use of the detergents and (2) wasting a mass of labour. In addition, the common windows are in favor of fogging leading to low visibility. Thus, owing to photocatalytic and photoinduced hydrophilic properties, semiconductor photocatalysts are widely and frequently employed to treat pollutants and withstand fogs. For these photocatalysts, titania (TiO<sub>2</sub>) is one of the most active and stable, arousing tremendous interests of many researchers. [21–24] Usually, crystalline TiO<sub>2</sub> exists in three different polymorphs: rutile (tetragonal), anatase (tetragonal) and brookite (orthorhombic). [25,26] Rutile TiO<sub>2</sub> (TiO<sub>2</sub>(R)) is a thermodynamically stable phase at all temperatures and the most common natural form of TiO<sub>2</sub>. Due to similar lattice parameters, TiO<sub>2</sub>(R) films are acted as buffer layer and growth template of VO<sub>2</sub>(M) films. [17] Nevertheless, TiO<sub>2</sub>(R) films are less efficient photocatalysts than anatase TiO<sub>2</sub> (TiO<sub>2</sub>(A)) films, which occupy an important position in the studies of photocatalytic active.

As mentioned above, it is reasonably hypothesized that the materials consisting of VO<sub>2</sub> and TiO<sub>2</sub> by the composites of compositions and the multilayer structure would simultaneously present antifogging, self-cleaning and energy-saving effects. This proposed material is a thrilling concept and of great value for applications in buildings. Frankly, a VO<sub>2</sub>/TiO<sub>2</sub> composite film has been prepared by atmospheric pressure CVD and introduced both photocatalytic and thermochromic properties. [27] However, the composite film reveals the graded distribution of surface composition from rich TiO<sub>2</sub> on the left to rich VO<sub>2</sub> on the right, which results in an unsatisfied combinatorial property. In addition, in 2003, to improve luminous transmittance of the VO<sub>2</sub> film, Jin et al. [1] have designed a TiO<sub>2</sub>(R)/VO<sub>2</sub>(M)/TiO<sub>2</sub>(R) multilayer film, where both TiO<sub>2</sub> layers are only applied its antireflection

effect. Subsequently, the work reported by Evans et al. [28] has dedicated to the fabrication of TiO<sub>2</sub>(A)/VO<sub>2</sub>(M) multilayer film and to the exploration of photocatalytic and thermochromic properties. But this film shows a low solar/heat control and a high contact angle (CA) with water. Therefore, to meet the requirements of application, some new innovations over the TiO<sub>2</sub>/VO<sub>2</sub>-based multilayer film are required.

Based on the above introduction, we propose a concept for constructing a TiO<sub>2</sub>(R)/VO<sub>2</sub>(M)/TiO<sub>2</sub>(A) multilayer film with antifogging, self-cleaning and energy-saving effects. As the buffer layer and the growth template of VO<sub>2</sub>(M) layer, bottom TiO<sub>2</sub>(R) layer with (1 1 0) orientation is a tetragonal form for VO<sub>2</sub>(M) layer with the less lattice mismatch (3.6%) [29] and restrains the Ca<sup>2+</sup> and Na<sup>+</sup> of flat glass diffusing into VO<sub>2</sub>(M) layer during the deposition process. Besides, TiO<sub>2</sub>(R) layer can increase the luminous transmittance ( $T_{lum}$ ) as antireflection layer because of its high transmittance. Then we successfully obtained localized epitaxial growth of VO<sub>2</sub>(M) layer on TiO<sub>2</sub>(R) layer at 300 °C of deposition temperature. Following top TiO<sub>2</sub>(A) layer with a graded structure was deposited on the VO<sub>2</sub>(M) layer. The graded structure from amorphous to crystalline can prevent the epitaxial growth of top TiO<sub>2</sub> layer on VO<sub>2</sub>(M) layer. It is pointed out by other researchers that the optimal photocatalytic performances are reached in a TiO<sub>2</sub> film with a mixed phase, in which anatase phase is predominant. [30] Thus a suitable amount of rutile TiO<sub>2</sub> is incorporated into the top TiO<sub>2</sub>(A) layer to improve the photocatalytic and photoinduced hydrophilic properties. In addition, to measure the multilayer film for application in smart window, we used a large-size MS apparatus with medium frequency pulsed power to deposit large-scale TiO<sub>2</sub>(R)/VO<sub>2</sub>(M)/TiO<sub>2</sub>(A) multilayer film. MS method can afford large areas for industrial purposes due to the advantages below: good adhesion of deposited films on substrates, excellent thickness uniformity, precise compositional control and long-term stability of the deposition process [31].

In this article, we report for the first time preparation of large-scale (400 × 400 mm<sup>2</sup> area) TiO<sub>2</sub>(R)/VO<sub>2</sub>(M)/TiO<sub>2</sub>(A) multilayer film at glass substrate as smart window for building applications. This film performed triple functions: thermochromism from the middle VO<sub>2</sub>(M) layer for solar energy modulation, photocatalytic and photoinduced hydrophilic properties from the top TiO<sub>2</sub>(A) layer for antifogging and self-cleaning effects. Furthermore, it was worth noting that the TiO<sub>2</sub> layers with a proper thickness could increase the  $T_{lum}$  of the film and enhance the regulation ability of the film for solar energy.

## Experimental section

### Sample preparation

The n-type Si (1 0 0) and the flat glasses with 400 × 400 mm<sup>2</sup> area were applied as the substrates. TiO<sub>2</sub>(R)/VO<sub>2</sub>(M)/TiO<sub>2</sub>(A) multilayer film was deposited using medium frequency reactive MS (MFRMS) system to sputter planar rectangular metal targets (purity > 99.5 wt.%, 610 × 85 mm<sup>2</sup> of area) in Ar (99.99%) and O<sub>2</sub> (99.99%) mixed atmosphere. Using a load-lock system, the base pressure of the deposition chamber was kept at 5.0 × 10<sup>-4</sup> Pa. Thereafter, the power was charged on the metal target with injection of mixed

**Table 1** Deposition conditions of each layer to produce the multilayer film.

Layer	Work current (A)	Work voltage (V)	Time (min)	Deposition pressure (Pa)	Deposition temperature (°C)	Ar flow rate (sccm)	O <sub>2</sub> flow rate (sccm)
TiO <sub>2</sub> (R)	20	620	30	0.4	300	12	28
VO <sub>2</sub> (M)	3	640	40	0.8	300	72	5
TiO <sub>2</sub> (A)	4	535	4	1.3	below 100	56	131
	8	555	3				
	12	567	3				
	16	587	80				

gas and the layer/film was deposited. On the basis of a series of studies by our group, [24,32-35] details of the deposition conditions of each layer are listed in Table 1. As shown in Table 1, the graded structure of TiO<sub>2</sub>(A) layer from amorphous to crystalline was realized by step by step process for increasing the work current of TiO<sub>2</sub>(A) layer. The initial amorphous structure was designed to prevent the epitaxial growth of top TiO<sub>2</sub> layer on VO<sub>2</sub>(M) layer.

### Film characterization

X-ray diffraction (XRD) was applied to characterize the crystalline structure of the films using a Rigaku Ultima IV diffractometer with grazing angle mode using Cu K $\alpha$  radiation ( $\lambda=0.15418$  nm). Fourier transformed infrared (FTIR) spectroscopy at a grazing angle of 80° (Thermo-Nicolet is10 Fourier spectrometer equipped with variable angle reflection accessory), 800 scans and 4 cm<sup>-1</sup> resolution, was used to analyse the organic contamination of the film surface. The root-mean-square (RMS) roughness of the films was obtained using atomic force microscopy (AFM, SII Nano Technology Ltd, Nanonavi II) in tapping mode. Unless stated otherwise, the RMS roughness of the multilayer film was calculated three times at a different spot with 3 × 3 μm<sup>2</sup> area. Aiming to determine the microstructure of the film, field emission scanning electron microscopy (FESEM, Magellan 400) and high-resolution transmission electron microscopy (TEM, Tecnai G2 F20 S-Twin) were employed to observe the surface and cross section of the multilayer film.

### Evaluation of energy-saving effect

The optical transmittance characteristics were monitored using a Hitachi U-3010 UV-visible-near-IR spectrophotometer at normal incidence from 250 to 2600 nm with an incorporated heating stage. The spectra of the multilayer film were taken at 25 and 90 °C, corresponding to VO<sub>2</sub>(M) and VO<sub>2</sub>(R), respectively. For the multilayer film, the integrated luminous transmittance ( $T_{lum}$ , 380-780 nm) and solar transmittance ( $T_{sol}$ , 240-2600 nm) were acquired from the recorded spectra using the following equation:

$$T_i = \int \phi_i(\lambda)T(\lambda)d\lambda / \int \phi_i(\lambda)d\lambda \quad (1)$$

where  $T(\lambda)$  is the transmittance at wavelength  $\lambda$ ,  $i$  luminous or solar for calculations,  $\phi_{lum}$  the standard luminous efficiency function for photopic vision, and  $\phi_{sol}$  the solar irradiance spectrum for an air mass of 1.5 (corresponding to the sun

standing 37° above the horizon). In addition, the optical transition behaviour was studied by recording the IR transmittance at 2000 nm against temperature with a heating-cooling rate of 2 °C/min, and a transition temperature  $T_c$  was defined as the temperature at the half-maximum on the heating curve, as has been described in an earlier article[36].

### Contact angle measurements

The wettability of the TiO<sub>2</sub>(R)/VO<sub>2</sub>(M)/TiO<sub>2</sub>(A) multilayer film was determined by measuring the CA of a water droplet on the film surfaces. The method of digital video image was used to process the sessile droplets by a contact angle apparatus (Chengde Dingsheng Testing Machine Co. Ltd, JY-82A). A CCD camera with space resolution 1280 × 1024 and color resolution 256 Gy levels was applied to capture the droplet images. A deionized water droplet was injected onto the surface using a 1 mL micro-injector. Typical time, necessary for equilibrating the initial shape of water droplet, did not exceed milliseconds, and thus we referred to the angle obtained in 2 s after the droplet deposition, as an initial contact angle. [37] The measured initial contact angles, as follows from the behaviour of contact diameter, corresponded to advancing contact angles. Subsequent evolution of droplet shape was determined by pinning of contact line in droplet spreading over rough surfaces. However, the flat film surface (RMS < 5.5 nm) could give rise to little evolution of droplet shape, as shown in the manuscript. [34] The water contact for each film before or after UV light irradiation (produced by a Xe lamp with 300 W power and wavelength range from 250 to 2000 nm) was averaged from five measurements. The multilayer film after UV light irradiation was further stored in an open vessel to observe the time-dependent evolution of contact angle. To examine the antifogging effect, the multilayer film was cooled at about -15 °C for 30 min in a refrigerator, and exposed to a constant and humid laboratory conditions (25 °C and relative humidity of 45%).

### Photocatalytic activity

Prior to all tests of photocatalytic activity, the multilayer film was irradiated by UV lights for 2 h to decompose pollutants adsorbed on the surface. The photocatalytic activity of the multilayer film was measured against a stearic acid overlayer, which was formed by drop-casting a saturated methanolic solution and drying in an oven at 60 °C for 30 min. The photodegradation of the stearic acid overlayer was

conducted by irradiating with UV lights, monitoring the CA of the film surface and the adsorption intensity of IR spectrum by using the FTIR spectroscopy versus irradiation time.

An amount of 0.5 mL of a 0.01 M rhodamine B (RhB) aqueous solution was diluted to 100 mL with deionized water, and then the diluted solution was stirred under darkness for 2 h to achieve adsorption-desorption equilibrium. Subsequently, the solution was injected into a small-size container with a hollow volume of  $2.5 \times 2.5 \times 1.0 \text{ cm}^3$  using a 5 mL injector. A similar schematic diagram of the degradation experiments has been shown in previous work. [24] At given irradiation intervals (30 min), the adsorption spectrum of the RhB solution was obtained with an UV-visible spectrometer at wavelengths from 650 to 400 nm. The concentration of RhB was determined by monitoring the changes in the absorbance maximum at about 500 nm. According to the Lambert-beer law, the absorbance is proportional to the concentration of a dilute solution, from which the photodegradation percentage could be calculated using the formula:

$$\eta = \frac{C_0 - C}{C_0} \times 100\% \quad (2)$$

where  $\eta$  denotes the degradation rate,  $C_0$  the initial concentration of the RhB solution and  $C$  the concentration at a certain irradiation time.

## Results and discussion

### Microstructure

TiO<sub>2</sub>(R)/VO<sub>2</sub>(M)/TiO<sub>2</sub>(A) multilayer film was prepared on a large-scale glass with area of  $400 \times 400 \text{ mm}^2$  using magnetron sputtering method, as shown in Fig. 1a. The multilayer film is homogeneous and brown-yellow in color. Fig. 1b displays XRD patterns of monolayer (TiO<sub>2</sub>(R), VO<sub>2</sub>(M) and TiO<sub>2</sub>(A)), bilayer (TiO<sub>2</sub>(R)/VO<sub>2</sub>(M)) and multilayer (TiO<sub>2</sub>(R)/VO<sub>2</sub>(M)/TiO<sub>2</sub>(A)) films, respectively. The deposition conditions of the monolayer and bilayer films were in line with that of the multilayer film. By comparing our results with Powder Diffraction File cards [38], it was evident that TiO<sub>2</sub>(R) and TiO<sub>2</sub>(A) films were pure rutile phase and mixed phase with dominant anatase phase, respectively. An estimation of the anatase content in the TiO<sub>2</sub>(A) film, as developed by Spurr and Myers [39], was made using the following equation:

$$f_A = \frac{1}{1 + 1.26(I_R/I_A)} \quad (3)$$

where  $f_A$  is the weight fraction of anatase and  $I_R$  and  $I_A$  are the intensities of rutile (1 1 0) and anatase (1 0 1), respectively. In the light of Eq. (3) and the values of  $I_R$  and  $I_A$  obtained by Jade 5 data analysis software,  $f_A$  reaches up to 0.95 in the film. Furthermore, it was easily observed that the VO<sub>2</sub> monolayer film presented a bad crystallinity without existence of M phase. This result can be attributed to the diffusion of Ca<sup>2+</sup> and Na<sup>+</sup> of flat glass into the VO<sub>2</sub> film and the requirement of higher temperature (> 400 °C) to crystallize the VO<sub>2</sub> film [40]. However, for the TiO<sub>2</sub>/VO<sub>2</sub> film, the mixed phase of vanadium oxide was found in the top VO<sub>2</sub> layer, which consisted primarily of M phase, another

monoclinic phase (B phase) [41] and tetragonal phase (A phase) [42] of VO<sub>2</sub>. The peaks assignable to VO<sub>2</sub>(M) were those at 27.86°, 33.34°, 36.98°, 42.27° and 55.45°. The characteristic peaks of VO<sub>2</sub>(A) and VO<sub>2</sub>(B) were at 25.46° and 26.27°, respectively, while the other peaks were assigned to the phases of V<sub>6</sub>O<sub>13</sub> and V<sub>2</sub>O<sub>5</sub>. Finally, in this article, the VO<sub>2</sub> layer with mixed phase was presented as VO<sub>2</sub>(M). There are some reasons for explaining the mixed phase of VO<sub>2</sub> layer. First of all, due to lack of covering layer, the VO<sub>2</sub> is liable to be oxidized to VO<sub>x</sub> ( $x > 2$ ). [43] In addition, the bottom TiO<sub>2</sub>(R) layer deposited at low temperature can possess imperfect crystalline region leading to formation of other phases, namely, the growth of M phase of VO<sub>2</sub> layer on the TiO<sub>2</sub>(R) layer is localized epitaxial. As shown in Fig. 1b, XRD pattern of TiO<sub>2</sub>(R)/VO<sub>2</sub>(M)/TiO<sub>2</sub>(A) multilayer film simultaneously reflected the information of the phase structure of the top TiO<sub>2</sub>(A) layer and middle VO<sub>2</sub>(M) layer. The diffraction peaks of V<sub>6</sub>O<sub>13</sub> and V<sub>2</sub>O<sub>5</sub> were hardly found in XRD pattern of the multilayer film, in contrast to that of TiO<sub>2</sub>(R)/VO<sub>2</sub>(M) film. This result can be ascribed to weak signals of these peaks and the presence of antioxidation of TiO<sub>2</sub>(A) layer. FESEM image of fractured cross-section of the multilayer film is displayed in Fig. 1c. The thickness of the multilayer film was about 440 nm, which made up of 100 nm TiO<sub>2</sub>(R) layer, 150 nm VO<sub>2</sub>(M) layer and 190 nm TiO<sub>2</sub>(A) layer. Obviously, VO<sub>2</sub>(M) layer showed loose and porous structure, while both TiO<sub>2</sub> layer were compact and dense. It is demonstrated by their surface morphology (in the insets of Fig. 1c) that the surface of VO<sub>2</sub>(M) layer derived from TiO<sub>2</sub>(R)/VO<sub>2</sub>(M) bilayer film was plain structure with cracks and pores. The presence of the cracks and pores should be expected to enhance the thermochromic performance of VO<sub>2</sub>(M) layer. [44] In addition, the surface of top TiO<sub>2</sub>(A) layer owned high nonequilibrium nano grain boundaries, which can increase the adsorption capacity of the film surface. [34] HRTEM study was done on the multilayer film with much attention devoted to the interface between TiO<sub>2</sub>(R) layer and VO<sub>2</sub>(M) layer, as exhibited in Fig. 1d. The spacing of the lattice fringes was around 0.325 and 0.319 nm in the TiO<sub>2</sub>(R) layer and VO<sub>2</sub>(M) layer, which could be indexed as the (1 1 0) plane of rutile and (0 1 1) plane of M phase, respectively. On account of existence of other phases in VO<sub>2</sub>(M) layer, we express such growth, that is, the preferential growth of VO<sub>2</sub>(M) lattice as the extension of crystal structure of TiO<sub>2</sub>(R) grains, as localized epitaxial growth. The localized epitaxy presents a growth relationship with  $[0 1 1]_{\text{VO}_2(\text{M})} // [1 1 0]_{\text{TiO}_2(\text{R})}$ , as a reasonable result of the great similarity of the two materials in crystal structure.

### Energy-saving effects

Fig. 2a and Table 2 depict the optical properties of TiO<sub>2</sub>(R)/VO<sub>2</sub>(M)/TiO<sub>2</sub>(A) multilayer film in response to different ambient temperature (25 °C and 90 °C), in comparison to that of TiO<sub>2</sub>(R)/VO<sub>2</sub>(M) bilayer film. Spectral transmittance of TiO<sub>2</sub>(R)/VO<sub>2</sub>(M)/TiO<sub>2</sub>(A) and TiO<sub>2</sub>(R)/VO<sub>2</sub>(M) films on the large-scale glasses measured by the spectrophotometer is almost accord with the spectra obtained by computational simulation with normal optical parameters (shown in Supporting Information). It is clearly manifested in Table 2 that  $\Delta T_{\text{sol}}$  (10.2%) of the multilayer film was reasonably improved and its  $T_{\text{lum}}$  was nearly constant, compared with

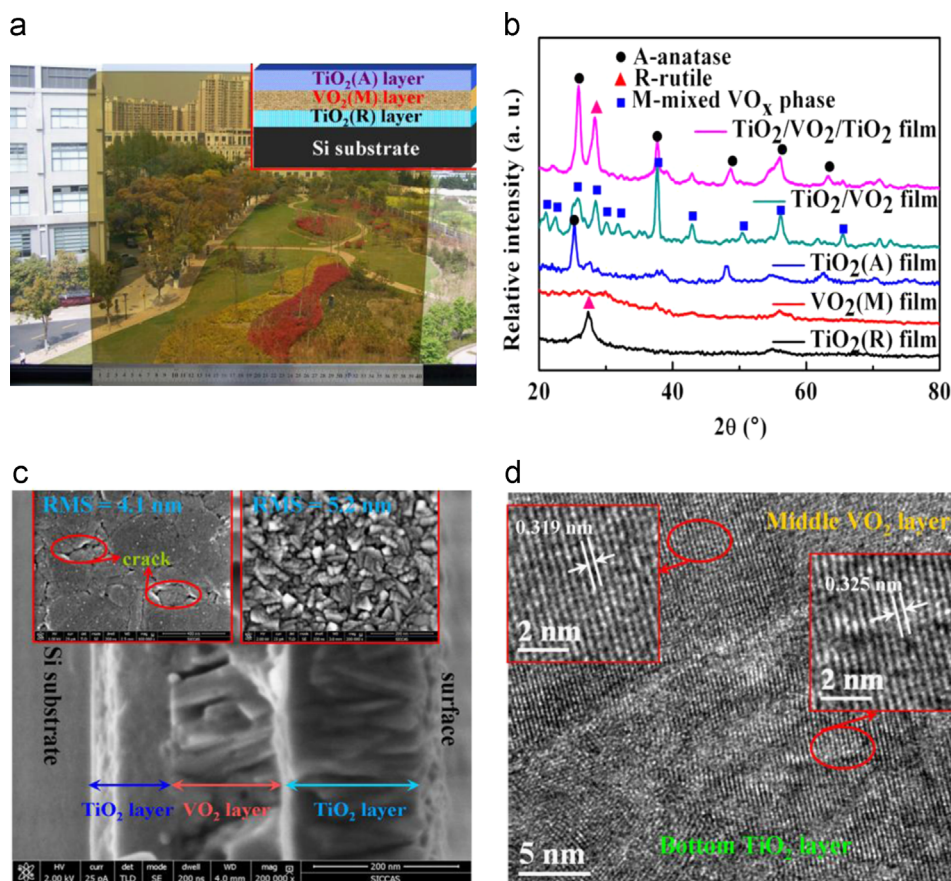


**Fig. 1** (a) Photograph of large-scale ( $400 \times 400 \text{ mm}^2$  area) multilayer film at room temperature (the inset is corresponding structure diagram of the multilayer film). (b) XRD patterns of monolayer ( $\text{TiO}_2(\text{R})$ ,  $\text{VO}_2(\text{M})$  and  $\text{TiO}_2(\text{A})$ ), bilayer ( $\text{TiO}_2(\text{R})/\text{VO}_2(\text{M})$ ) and multilayer ( $\text{TiO}_2(\text{R})/\text{VO}_2(\text{M})/\text{TiO}_2(\text{A})$ ) films. (c) FESEM image of fractured cross-section of the multilayer film (the insets are surface morphology of  $\text{VO}_2(\text{M})$  (left) and  $\text{TiO}_2(\text{A})$  layers (right), respectively). (d) HRTEM image of the interface between  $\text{TiO}_2(\text{R})$  layer and  $\text{VO}_2(\text{M})$  layer (the insets correspond to the red rings in the image with high magnification).

those of the bilayer film. The increase of  $\Delta T_{\text{sol}}$  could be expounded by the following two aspects. To begin with, the top  $\text{TiO}_2(\text{A})$  layer with a proper thickness (190 nm) is regarded as antireflection coating to reduce the reflectivity of the multilayer film. According to the Sellmeier dispersion formula, [45] the decreased reflectivity would directly lead to the enhancement of the solar regulation efficiency. Besides, another role of  $\text{TiO}_2(\text{A})$  layer is as a protective layer to avoid or retard the oxidation of  $\text{VO}_2$  layer. Generally, the  $\text{VO}_x$  ( $x > 2$ ) hardly works under the testing conditions owing to a high phase-transition temperature ( $T_c > 100 \text{ }^\circ\text{C}$ ). [46] In addition, temperature dependence of the optical transmittance of the multilayer film at a fixed wavelength of 2000 nm is displayed in Fig. 2b. In the case, a metal-insulator transition (MIT) was obviously assessed to occur at about  $61.5 \text{ }^\circ\text{C}$ , which is lower than  $T_c = 68 \text{ }^\circ\text{C}$  reported by previous studies. [8,47] It is noticed that no action was deliberately taken for the reduction of  $T_c$ . We suggest at least the following reasons most probably responsible for the reduction of  $T_c$ . A slight deviation from stoichiometry, either under- or overstoichiometry, is known to reduce  $T_c$ . [48] Furthermore, the crystal defects (shown in Fig. 1c) may damage the zigzag chains of the V-V pairs characteristic of the low-temperature phase, resulting in the decrease of  $T_c$ . [49] And lastly, the tensile stress

(2.54 GPa, shown in Supporting Information) of the multilayer film can also devote to causing a  $T_c$  reduction [50].

To estimate the applied properties, the  $400 \times 400 \text{ mm}^2$  area of flat glass (3 mm in thickness) coated with  $\text{TiO}_2(\text{R})/\text{VO}_2(\text{M})/\text{TiO}_2(\text{A})$  multilayer film was employed in a model house (Fig. 2c) to survey roughly the regulation effect of infrared light. The house was made of some boards (15 mm thickness) painted on both sides for thermal insulation. The internal space of the house was about  $8.5 \times 10^7 \text{ mm}^3$  ( $550 \times 360 \times 430 \text{ mm}^3$ ). The glass with the multilayer film was placed in the front of the house as windows ( $390 \times 390 \text{ mm}^2$ ), and the combination of the house and the window was sealed during the testing process. On the side, a house with a piece of blank glass was served as a control group at the identical test conditions, in comparison with the former. The separation distance of both houses was 90 mm. Two infrared lamps (PHILIPS, R125 IR R 150 W) irradiated the houses, while two thermoelectric couples were employed to monitor the temperature changes. Furthermore, two InGaAs PIN photodiodes (Hamamatsu Co., G8373-01), which sensed the changes of transmittance of infrared light (as shown in Fig. 2d), were installed in the small pores on the center of back panel of each model house. Initially, the experiment was conducted at  $13 \text{ }^\circ\text{C}$  without irradiation of infrared lamps. After 90 min of

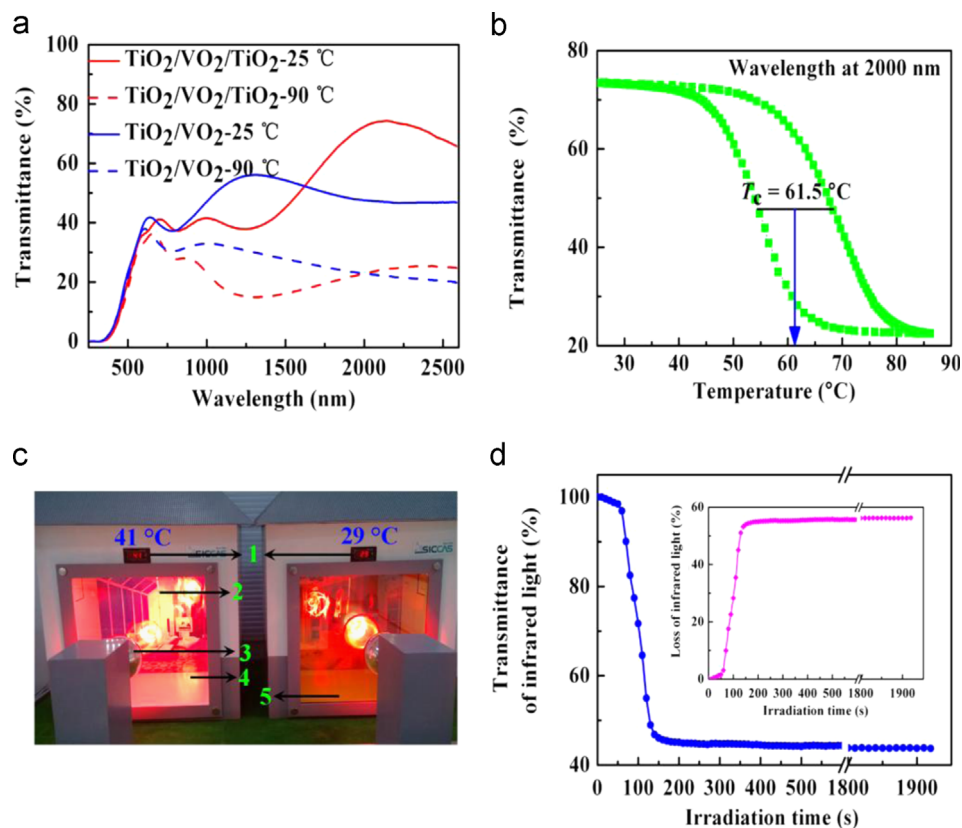


**Fig. 2** (a) Optical transmittance spectra of TiO<sub>2</sub>(R)/VO<sub>2</sub>(M)/TiO<sub>2</sub>(A) multilayer film and TiO<sub>2</sub>(R)/VO<sub>2</sub>(M) bilayer film at low and high temperature. (b) Temperature dependence of the optical transmittance of the multilayer film at a fixed wavelength of 2000 nm. (c) Photographic illustration of the testing system, 1: temperature monitor, 2: temperature probe, 3: infrared lamps, 4: blank glass, and 5: glass with TiO<sub>2</sub>(R)/VO<sub>2</sub>(M)/TiO<sub>2</sub>(A) multilayer film. (d) Transmittance of infrared light dependence on irradiation time for multilayer film (the inset is the infrared shielding ability of the multilayer film).

**Table 2** The solar energy control properties of TiO<sub>2</sub>(R)/VO<sub>2</sub>(M)/TiO<sub>2</sub>(A) multilayer film and TiO<sub>2</sub>(R)/VO<sub>2</sub>(M) bilayer film.

Film	$T_{\text{sol-L}}$ (%)	$T_{\text{sol-H}}$ (%)	$\Delta T_{\text{sol}}$ (%)	$T_{\text{lum-L}}$ (%)	$T_{\text{lum-H}}$ (%)	$\Delta T_{2000}$ (%)
TiO <sub>2</sub> /VO <sub>2</sub> /TiO <sub>2</sub>	33.8	23.6	10.2	30.1	27.8	49.5
TiO <sub>2</sub> /VO <sub>2</sub>	37.2	28.6	8.6	32.4	31.3	24.6

irradiation, it is clearly indicated in Fig. 2c that the application of the multilayer film causes a temperature reduction of 12 °C compared with the blank glass (temperature of 41 °C). To further analyze the phenomenon, transmittance of infrared light dependence on irradiation time for multilayer film is shown in Fig. 2d. The transmittance (or loss) of infrared light for the multilayer film decreased (or increased) from 100 (0%) to 45.2% (54.8%) in response to irradiation time from 0 to 3 min. Afterwards, the transmittance of infrared light was almost constant value (43.7%). Therefore, the infrared shielding ability of TiO<sub>2</sub>(R)/VO<sub>2</sub>(M)/TiO<sub>2</sub>(A) multilayer film reaches up to 56.3% and is higher than that of TiO<sub>2</sub>(R)/VO<sub>2</sub>(M) film (39.7%, shown in Supporting Information).

### Wettability

Fig. 3a exhibits the influence of irradiation time of UV light on the CAs of the surface of TiO<sub>2</sub>(R)/VO<sub>2</sub>(M)/TiO<sub>2</sub>(A) multilayer

film. When the irradiation time was 5 min, the static water CAs of the multilayer film reduced abruptly from 86.4° (hydrophobicity) [51] to 6.4° (hydrophilicity). Along with the irradiation time being extended to 10 min, the wettability of the multilayer film transformed into superhydrophilicity (CA < 5°). [52,53] However, it should be mentioned that the multilayer film performed more sensitive photoinduced hydrophilicity and lower CA than TiO<sub>2</sub>(A) single film (CA > 5°, shown in Supporting Information). The sandwich structure of the multilayer film can be responsible for the excellent photoinduced action because of effective separation of photogenerated electrons and holes. [54] Moreover, on account of Wenzel equation, [55] the multilayer film has more rough surface giving rise to lower CA, in contrast to the TiO<sub>2</sub>(A) single film (shown in Supporting Information). As shown in Fig. 3a, the water droplet shape on the multilayer film surface was hydrophobicity before UV irradiation. Usually, the wettability of materials is governed by both the chemical composition and the structure of solid surfaces. In Fig. 1c, RMS of the multilayer film was 5.2 nm,

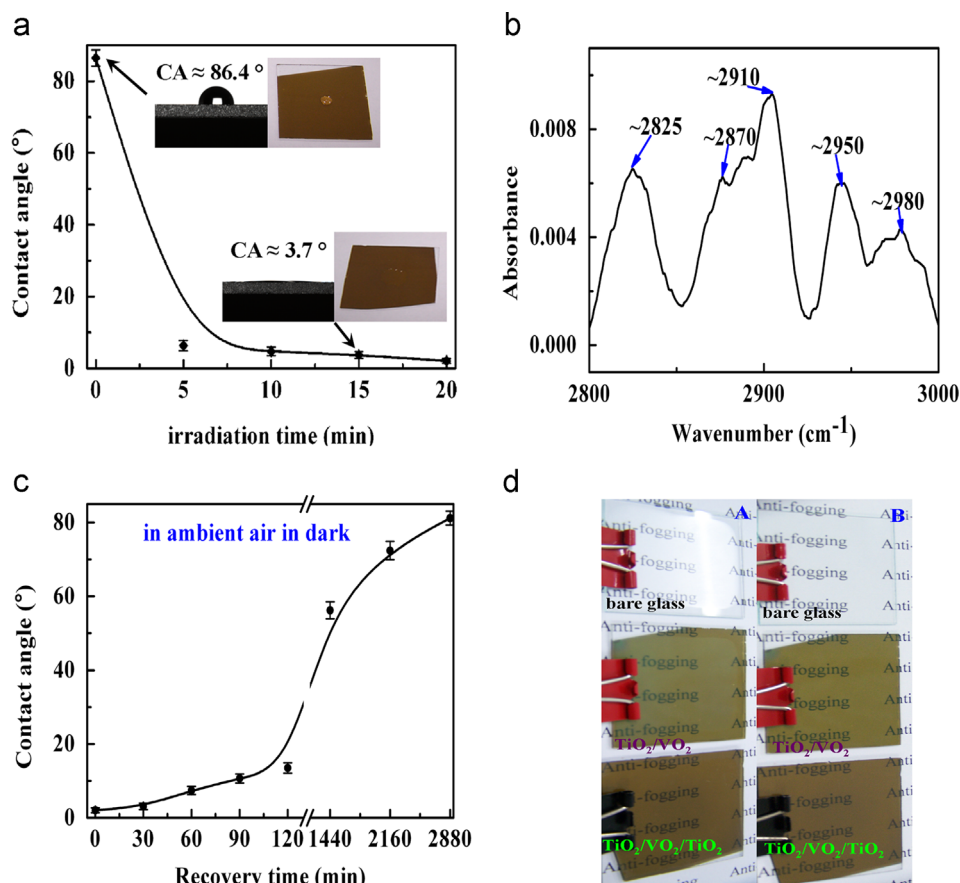


**Fig. 3** (a) Effect of irradiation time of UV light on the CAs of the surface of  $\text{TiO}_2(\text{R})/\text{VO}_2(\text{M})/\text{TiO}_2(\text{A})$  multilayer film (the insets show relevant water droplet shapes on the film surface and their optical images). (b) IR absorbance spectrum of the multilayer film. (c) Time-dependent evolution of CA for the multilayer film exposed to ambient air in dark. (d) Photographs of a naked glass (upper) and both glasses coated with  $\text{TiO}_2(\text{R})/\text{VO}_2(\text{M})$  (middle) and  $\text{TiO}_2(\text{R})/\text{VO}_2(\text{M})/\text{TiO}_2(\text{A})$  (bottom) films before (B) and after (A) cooled below  $-15^\circ\text{C}$  for 30 min in a refrigerator followed by exposure to humid laboratory air.

making known the relatively flat surface. For the flat surface of  $\text{TiO}_2$ , the origin of hydrophobicity is identified as fully stoichiometric  $\text{TiO}_2$  and hydrocarbon adsorbates on the film surface reported in our previous work. [34] To confirm the adsorption of organic contaminants on the surface, infrared (IR) absorption section spectrum (Fig. 3b) was measured at a grazing angle of  $80^\circ$ . The characteristic alkyl C–H bond stretching vibrations of  $\text{CH}_2$  and  $\text{CH}_3$  groups were ubiquitous detected from the multilayer film in the range  $3000\text{--}2800\text{ cm}^{-1}$ . [37] This result provides a direct evidence for the hydrocarbon contaminants existing in the multilayer film surface. In addition, the chemical composition of the multilayer film surface was determined by X-ray photoelectron spectroscopy (XPS). The  $\text{Ti } 2p_{3/2}$  spectrum of the multilayer film (show in Supporting Information) only had a peak at 458.8 eV, which was assigned to  $\text{Ti}^{4+}$ . [56] Thus, the surface of  $\text{TiO}_2(\text{R})/\text{VO}_2(\text{M})/\text{TiO}_2(\text{A})$  multilayer film is approximate fully oxidized or free oxygen vacancy.

After UV irradiation, we subjected the  $\text{TiO}_2(\text{R})/\text{VO}_2(\text{M})/\text{TiO}_2(\text{A})$  multilayer film to ambient air in dark, as displayed in Fig. 3c. Apparently, CAs of the multilayer film increased gradually from  $\sim 0$  to  $\sim 80^\circ$  when the multilayer film was stored in dark within 2 days. This result implies that the wettability of the multilayer film returns to hydrophobic in the air again, and the cycles of hydrophobicity and superhydrophilicity is repeated by alteration of external circumstances. It

should be noted that the multilayer film maintained in superhydrophilicity ( $\text{CA} < 5^\circ$ ) in 30 min exposure time under the ambient air. As mentioned above, a combined action of fully stoichiometric  $\text{TiO}_2$  of the multilayer film surface and adsorbates with low surface energy on the surface can yield a hydrophobic surface. In regard to the mechanism of the reversible conversion of hydrophobic to superhydrophilic, both factors should be considered in the reaction process. When the multilayer film is irradiated by UV light, the film surface rapidly generates the oxygen vacancies at bridging sites of the film surface, resulting in the conversion of relevant  $\text{Ti}^{4+}$  sites to  $\text{Ti}^{3+}$  sites. These defects react with water molecules to form hydrophilic domain ( $-\text{OH}$ ) and improve the surface hydrophilicity greatly. [51,57–59] Meanwhile, hydrocarbon adsorbates on the film surface are decomposed under UV irradiation, which further decrease the CA of the film. [37,60] Subsequently, the multilayer film surface exposed to the ambient air in dark, which is an energetically metastable state, [61] needs to reabsorb the atmospheric oxygen and organic contaminants to reduce the Gibbs free energy of the film and be hydrophobic. The superhydrophilicity generally brings about an antifogging effect, which may be demonstrated by exposing the coated or bare glasses to humid environments after cooling it at a low temperature (below  $-15^\circ\text{C}$ ). The photographs in

Fig. 3d exhibit that the naked glass (upper left of the Fig. 3d) and the glass with TiO<sub>2</sub>(R)/VO<sub>2</sub>(M) film (middle left of the Fig. 3d) immediately fogged to scatter light whereas the glass with TiO<sub>2</sub>(R)/VO<sub>2</sub>(M)/TiO<sub>2</sub>(A) multilayer film (bottom left of the Fig. 3d) remained original transparence after cooled below  $-15\text{ }^{\circ}\text{C}$  for 30 min followed by exposure to humid laboratory air.

### Self-cleaning function

Self-cleaning property of TiO<sub>2</sub>(R)/VO<sub>2</sub>(M)/TiO<sub>2</sub>(A) multilayer film was evaluated by the decomposition of stearic acid under UV light. The degradation of stearic acid was related to the decrease in IR absorption of the C–H stretches. [62] Fig. 4a summarizes IR absorbance spectra of TiO<sub>2</sub>(R)/VO<sub>2</sub>(M)/TiO<sub>2</sub>(A) multilayer film with stearic acid overlayer at various irradiation time under UV light. Before UV light irradiation, the characteristic alkyl C–H bond stretching vibrations

of CH<sub>2</sub> and CH<sub>3</sub> groups ( $3000\text{--}2800\text{ cm}^{-1}$ ) were distinctly detected from the multilayer film surface. It is observed that the absorbance of alkyl C–H bond stretching vibrations decreased drastically after UV light irradiation of 20 min,

which means that a considerable proportion of stearic acid overlayer was decomposed. Whereafter, the IR absorbance slowly became weak with the increase of irradiation time, and finally almost faded away after 180 irradiation time. In addition, to further acquire precisely information for the degradation of stearic acid overlayer, we also studied the CAs of the multilayer film with stearic acid overlayer dependence on irradiation time (Fig. 4b). As acknowledged widely, the stearic acid is frequently used for surface modification of other materials to produce hydrophobic or superhydrophobic surface due to its low surface energy. In Fig. 4b, the multilayer film with stearic acid overlayer was hydrophobic and its CA ( $\sim 99.5^{\circ}$ ) was higher than that of untreated multilayer film ( $\text{CA} \approx 86.4^{\circ}$ ). The CAs on the surface decreased from 99.5 to  $11.5^{\circ}$  in response to the changes of irradiation time from 0 to 180 min. The fact that the surface transforms from hydrophobic to hydrophilic should be ascribed to the degradation of stearic acid overlayer and the photoinduced hydrophilicity of multilayer film. Under UV irradiation, the change trend of CAs, which could be similar to the variation of IR absorption, was faster reduction at the initial stage and slower reduction in the rest of time. However, after 180 min UV irradiation, the multilayer film surface still had the presence of residual stearic acid, because the CA ( $=11.5^{\circ}$ ) was higher than  $5^{\circ}$ .

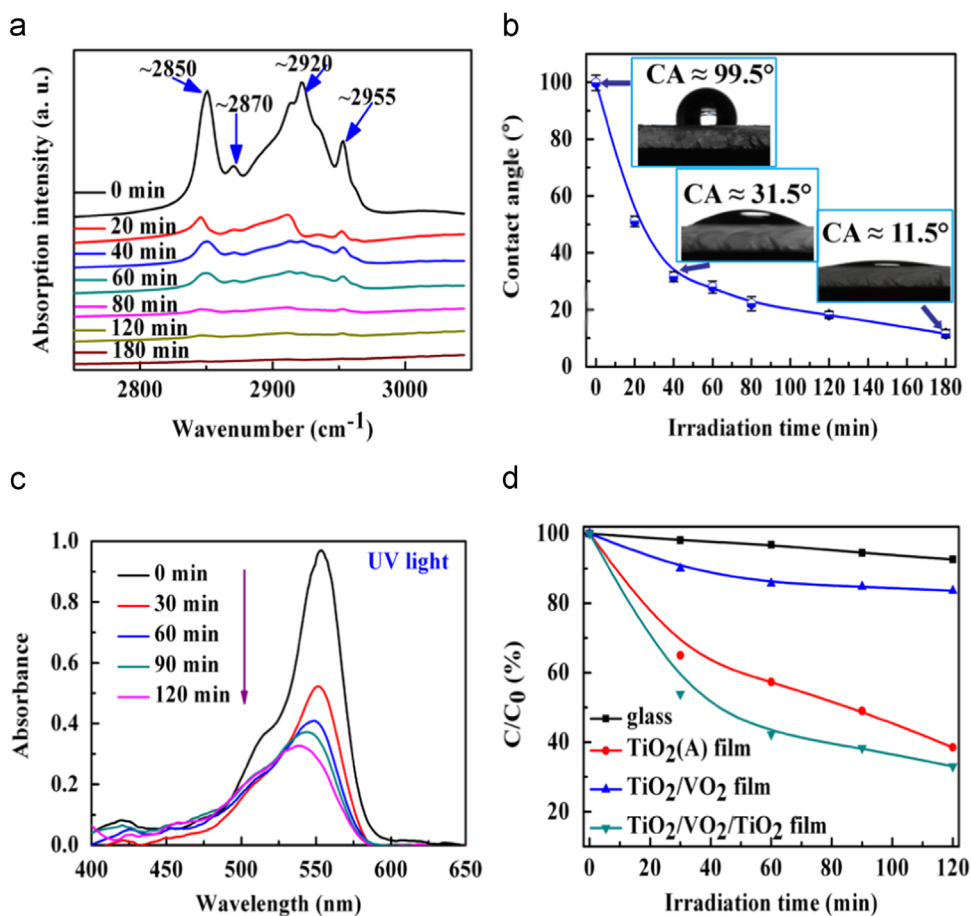


Fig. 4 (a) IR absorbance spectra of TiO<sub>2</sub>(R)/VO<sub>2</sub>(M)/TiO<sub>2</sub>(A) multilayer film with stearic acid overlayer at various irradiation time under UV light. (b) CAs of the multilayer film with stearic acid overlayer dependence on irradiation time (the insets are corresponding water droplet shapes on the surface). (c) Variation of absorbance spectra of RhB aqueous solution degraded by the multilayer film. (d) Photodegradation of RhB aqueous solution over the films (TiO<sub>2</sub>(A), TiO<sub>2</sub>(R)/VO<sub>2</sub>(M), and TiO<sub>2</sub>(R)/VO<sub>2</sub>(M)/TiO<sub>2</sub>(A)) under UV light ( $C_0$  is the initial concentration of RhB,  $C$  the concentration of RhB after irradiation).

The decomposition rate of RhB under UV light irradiation was another way to assess the photocatalytic activity of TiO<sub>2</sub>(R)/VO<sub>2</sub>(M)/TiO<sub>2</sub>(A) multilayer film. Fig. 4c presents the absorption spectra of RhB aqueous solution degraded by the multilayer film under UV light irradiation. The decrease of the absorbance for the primary peak at around 550 nm means the degradation of RhB. As shown in Fig. 4c, after 120 min of illumination, this peak had an obvious reduction. It is worth to declare that the decomposition of RhB was completely translated to final products, and not to intermediate species (N-deethylation of RhB). The peak of the intermediate species should be observed at about 500 nm. [63] On basis of Lambert-Beer law, the absorbance of RhB was transformed into the concentration appeared in Fig. 4d. It needs to be pointed out that a slight photodegradation of RhB was found on the surface of bare glass. Owing to more degradation of RhB, TiO<sub>2</sub>(R)/VO<sub>2</sub>(M)/TiO<sub>2</sub>(A) multilayer film had a better photocatalytic activity than TiO<sub>2</sub>(A) film. However, TiO<sub>2</sub>(R)/VO<sub>2</sub>(M) film decomposed a small amount of RhB as a result of adsorption by loose structure of the surface (e.g. cracks and pores, as shown in Fig. 1c).

It is well known that the activity of a photocatalytic film is dependent upon its four physical properties: bandgap energy, crystallinity, surface roughness and film thickness. [64] The decent photocatalytic activity of TiO<sub>2</sub>(R)/VO<sub>2</sub>(M)/TiO<sub>2</sub>(A) multilayer film should be resulted from wide bandgap of TiO<sub>2</sub>(A) layer (3.35 eV, shown in Supporting Information) and relatively high film thickness (440 nm). The efficiency of photocatalysis strongly depends on the lifetime of electron-hole pairs generated by electronic excitation, and the recombination probability is inversely proportional to the magnitude of the band gap. [65] Thus a large bandgap can prolong the lifetime of electron-hole pairs to enhance the photocatalytic activity of the multilayer film. On the other hand, it is demonstrated by previous studies that there is a linear relationship with a high degree of correlation between film thickness and the level of UV light absorbed. [64] The thick film can increase the probability for photon absorption.

## Conclusion

A large-scale multifunctional TiO<sub>2</sub>(R)/VO<sub>2</sub>(M)/TiO<sub>2</sub>(A) multilayer film was deposited by MFRMS under a moderate deposition temperature. The bottom TiO<sub>2</sub>(R) layer, which only showed rutile phase with (1 1 0) orientation, played as the buffer layer and growth template of VO<sub>2</sub>(M) layer. The middle VO<sub>2</sub>(M) layer owned an excellent thermochromic property, and the top TiO<sub>2</sub>(A) layer displayed an eminent photoinduced hydrophilicity and a considerable photocatalytic activity. In short, the multilayer film incorporating into energy-saving, antifogging and self-cleaning effects can have a great potential application for smart windows.

## Acknowledgements

The authors are grateful to the high-tech project of MOST (2014AA032802), the national sci-tech support plan, the National Natural Science Foundation of China (NSFC, No.: 51032008, 51102270, 51272271).

## Appendix A. Supporting information

Supplementary data associated with this article can be found in the online version at <http://dx.doi.org/10.1016/j.nanoen.2014.09.023>.

## References

- [1] P. Jin, G. Xu, M. Tazawa, K. Yoshimura, *Appl. Phys. A* 77 (2003) 455-459.
- [2] C.G. Granqvist, *Thin Solid Films* 193 (1990) 730-741.
- [3] N.R. Mlyuka, G.A. Niklasson, C.G. Granqvist, *Sol. Energ. Mater. Sol. Cell* 93 (2009) 1685-1687.
- [4] Y.M. Li, S.D. Ji, Y.F. Gao, H.J. Luo, M. Kanehira, *Sci. Rep.-Uk* 3 (2013).
- [5] G.V. Jorgenson, J.C. Lee, *Sol. Energ. Mater* 14 (1986) 205-214.
- [6] S.M. Babulanam, T.S. Eriksson, G.A. Niklasson, C.G. Granqvist, *Sol. Energ. Mater* 16 (1987) 347-363.
- [7] Y. Gao, S. Wang, L. Kang, Z. Chen, J. Du, X. Liu, H. Luo, M. Kanehira, *Energ. Environ. Sci* 5 (2012) 8234.
- [8] F.J. Morin, *Phys. Rev. Lett.* 3 (1959) 34-36.
- [9] Y. Gao, C. Cao, L. Dai, H. Luo, M. Kanehira, Y. Ding, Z.L. Wang, *Energ. Environ. Sci* 5 (2012) 8708.
- [10] A.B. Huang, Y.J. Zhou, Y.M. Li, S.D. Ji, H.J. Luo, P. Jin, *J. Mater. Chem. A* 1 (2013) 12545-12552.
- [11] B.J. Kim, Y.W. Lee, B.G. Chae, S.J. Yun, S.Y. Oh, H.T. Kim, Y.S. Lim, *Appl. Phys. Lett.* 90 (2007) 023515.
- [12] Q.W. Shi, W.X. Huang, J. Wu, Y.X. Zhang, Y.J. Xu, Y. Zhang, S. Qiao, J.Z. Yan, *J. Appl. Phys.* 112 (2012) 033523.
- [13] A. Kafizas, G. Hyett, I.P. Parkin, *J. Mater. Chem.* 19 (2009) 1399-1408.
- [14] D. Vernardou, M.E. Pemble, D.W. Sheel, *Surf. Coat. Technol* 188 (2004) 250-254.
- [15] T.D. Manning, I.P. Parkin, M.E. Pemble, D. Sheel, D. Vernardou, *Chem. Mater.* 16 (2004) 744-749.
- [16] K. Nagashima, T. Yanagida, H. Tanaka, T. Kawai, *J. Appl. Phys.* 101 (2007) 026103.
- [17] K. Kawatani, H. Takami, T. Kanki, H. Tanaka, *Appl. Phys. Lett.* 100 (2012) 173112.
- [18] D. Ruzmetov, K.T. Zawilski, V. Narayanamurti, S. Ramanathana, *J. Appl. Phys.* 102 (2007) 113715.
- [19] C.H. Chen, Z.Y. Fan, *Appl. Phys. Lett.* 95 (2009) 262106.
- [20] Y. Zhao, J.H. Lee, Y.H. Zhu, M. Nazari, C.H. Chen, H.Y. Wang, A. Bernussi, M. Holtz, Z.Y. Fan, *J. Appl. Phys.* 111 (2012) 053533.
- [21] B. Kraeutler, A.J. Bard, *J. Am. Chem. Soc.* 100 (1978) 5985-5992.
- [22] O. Carp, C.L. Huisman, A. Reller, *Prog. Solid State Chem.* 32 (2004) 33-177.
- [23] Z. Liu, P.F. Fang, S.J. Wang, Y.P. Gao, F.T. Chen, F. Zheng, Y. Liu, Y.Q. Dai, *J. Mol. Catal. A-Chem.* 363 (2012) 159-165.
- [24] J. Zheng, S. Bao, Y. Guo, P. Jin, *Surf. Coat. Technol* 240 (2014) 293-300.
- [25] D.T. Cromer, K. Herrington, *J. Am. Chem. Soc.* 77 (1955) 4708-4709.
- [26] X. Bokhimi, A. Morales, M. Aguilar, J.A. Toledo-Antonio, F. Pedraza, *Int. J. Hydrogen Energ.* 26 (2001) 1279-1287.
- [27] M. Wilkinson, A. Kafizas, S.M. Bawaked, A.Y. Obaid, S.A. Al-Thabaiti, S.N. Basahel, C.J. Carmalt, I.P. Parkin, *ACS. Comb. Sci* 15 (2013) 309-319.
- [28] P. Evans, M.E. Pemble, D.W. Sheel, H.M. Yates, *J. Photochem. Photobiol. A-Chem.* 189 (2007) 387-397.
- [29] Y. Muraoka, Z. Hiroi, *Appl. Phys. Lett.* 80 (2002) 583-585.
- [30] B. Barrocas, O.C. Monteiro, M.E.M. Jorge, S. Serio, *Appl. Surf. Sci.* 264 (2013) 111-116.

- [31] K. Ellmer, *J. Phys. D-Appl. Phys* 33 (2000) R17-R32.
- [32] P. Jin, S. Nakao, S. Tanemura, T. Bell, L.S. Wielunski, M.V. Swain, *Thin Solid Films* 343 (1999) 134-137.
- [33] P. Jin, S. Nakao, S. Tanemura, *Thin Solid Films* 324 (1998) 151-158.
- [34] J.Y. Zheng, S.H. Bao, Y. Guo, P. Jin, *ACS Appl. Mater. Interface* 6 (2014) 1351-1355.
- [35] M. Jiang, S. Bao, X. Cao, Y. Li, S. Li, H. Zhou, H. Luo, P. Jin, *Ceram. Int.* 40 (2014) 6331-6334.
- [36] P. Jin, S. Tanemura, *Jpn. J. Appl. Phys.* 34 (1995) 2459-2460.
- [37] L.B. Boinovich, A.M. Emelyanenko, A.S. Pashinin, C.H. Lee, J. Drelich, Y.K. Yap, *Langmuir* 28 (2012) 1206-1216.
- [38] H.B. Weiser, W.O. Milligan, *J. Phys. Chem.Us.* 38 (1934) 513-519.
- [39] R.A. Spurr, H. Myers, *Anal. Chem.* 29 (1957) 760-762.
- [40] A. Rúa, R. Cabrera, H. Coy, E. Merced, N. Sepúlveda, F.I.E. Fernández, *J. Appl. Phys.* 111 (2012) 104502.
- [41] F. Théobald, R. Cabala, J. Bernard, *J. Solid State Chem.* 17 (1976) 431-438.
- [42] Y. Oka, T. Yao, N. Yamamoto, *J. Solid State Chem.* 86 (1990) 116-124.
- [43] Y.F. Gao, S.B. Wang, H.J. Luo, L. Dai, C.X. Cao, Y.L. Liu, Z. Chen, M. Kanehira, *Energ. Environ. Sci* 5 (2012) 6104-6110.
- [44] L. Kang, Y. Gao, H. Luo, Z. Chen, J. Du, Z. Zhang, *ACS. Appl. Mater. Interface.* 3 (2011) 135-138.
- [45] R.T. Kivaisi, M. Samiji, *Sol. Energ. Mater. Sol. Cell.* 57 (1999) 141-152.
- [46] S. Beke, *Thin Solid Films.* 519 (2011) 1761-1771.
- [47] Jb. Goodenou, *J. Solid State Chem.* 3 (1971) 490 (E).
- [48] Ch. Griffith, H.K. Eastwood, *J. Appl. Phys.* 45 (1974) 2201-2206.
- [49] A.R. Begishev, G.B. Galiev, A.S. Ignatev, V.G. Mokerov, V.G. Poshin, *Solid State Phys* 20 (1978) 1643-1650.
- [50] K. Okimura, T. Watanabe, J. Sakai, *J. Appl. Phys.* 111 (2012) 073514.
- [51] R. Wang, K. Hashimoto, A. Fujishima, M. Chikuni, E. Kojima, A. Kitamura, M. Shimohigoshi, T. Watanabe, *Nature* 388 (1997) 431-432.
- [52] X.T. Zhang, M. Jin, Z.Y. Liu, D.A. Tryk, S. Nishimoto, T. Murakami, A. Fujishima, *J. Phys. Chem. C.* 111 (2007) 14521-14529.
- [53] X.J. Feng, L. Feng, M.H. Jin, J. Zhai, L. Jiang, D.B. Zhu, *J. Am. Chem. Soc.* 126 (2004) 62-63.
- [54] M. Takahashi, K. Tsukigi, E. Dorjpalam, Y. Tokuda, T. Yoko, *J. Phys. Chem. B.* 107 (2003) 13455-13458.
- [55] R.N. Wenzel, *Ind. Eng. Chem* 28 (1936) 988-994.
- [56] D. Courcot, L. Gengembre, M. Guelton, Y. Barbaux, B. Grzybowska, *J. Chem. Soc. Faraday Trans.* 90 (1994) 895-898.
- [57] R. Wang, K. Hashimoto, A. Fujishima, M. Chikuni, E. Kojima, A. Kitamura, M. Shimohigoshi, T. Watanabe, *Adv. Mater.* 10 (1998) 135138.
- [58] N. Sakai, R. Wang, A. Fujishima, T. Watanabe, K. Hashimoto, *Langmuir* 14 (1998) 5918-5920.
- [59] Y. Sawai, S. Nishimoto, Y. Kameshima, E. Fujii, M. Miyake, *Langmuir* 29 (2013) 6784-6789.
- [60] L.G. Xu, J.H. He, L. Yao, *J. Mater. Chem. A.* 2 (2014) 402-409.
- [61] R. Wang, N. Sakai, A. Fujishima, T. Watanabe, K. Hashimoto, *J. Phys. Chem. B.* 103 (1999) 2188-2194.
- [62] A. Mills, J.S. Wang, *J. Photochem. Photobiol. A.* 182 (2006) 181-186.
- [63] Y. Ma, J.N. Yao, *J. Photochem. Photobiol. A.* 116 (1998) 167-170.
- [64] A. Kafzas, C.J. Carmalt, I.P. Parkin, *Chem. Eur. J* 18 (2012) 13048-13058.
- [65] T. Sumita, H. Otsuka, H. Kubota, M. Nagata, Y. Honda, R. Miyagawa, T. Tsurushima, T. Sadoh, *Nucl. Instrum. Method. Phys. Res* 148 (1999) 758-761.



**Jianyun Zheng** received his master's degree in Material Engineering from the Lanzhou Institute of Chemical Physics, Chinese Academy of Science, PR China in 2012. He is a Ph.D. candidate at the Shanghai Institute of Ceramics, Chinese Academy of Science, PR China. His research focuses on the energy saving materials, transition metal oxide films and devices for photocatalysts, spintronics and chromogenic materials.



**Shanhu Bao** received his Ph.D. Sci. degree in Graduate School of Science and Technology in Shinshu University. He is currently a professor/researcher at Shanghai Institute of Ceramics, Chinese Academy of Sciences. His research focuses on the energy saving materials, oxide-based electrochromic and thermochromic materials and devices, magnesium based thin film switchable mirror and hydrogen sensors.



**Jin Ping** received his Ph.D. degree from department of Electrical and Computer Engineering in Nagoya Institute of Technology, Japan in 1992. He is currently the director of the Research Center for Industrial Ceramics and the full professor of Shanghai Institute of Ceramics, Chinese Academy of Sciences. His research focuses on the energy saving materials, transition metal oxide films and devices for photocatalysts, optical and chromogenic materials.